Surface & Coatings Technology 258 (2014) 392–397

Contents lists available at ScienceDirect

Surface & Coatings Technology

journal homepage: www.elsevier.com/locate/surfcoat

Incorporation effects of Si in TiC_x thin films

O. Tengstrand [a,*], N. Nedfors [b], B. Alling [a], U. Jansson [b], A. Flink [a,c], P. Eklund [a], L. Hultman [a]

[a] Thin Film Physics Division, Department of Physics, Chemistry and Biology (IFM), Linköping University, SE-581 83 Linköping, Sweden
[b] Department of Chemistry, The Ångström Laboratory, Uppsala University, P.O. Box 538, SE-751 21 Uppsala, Sweden
[c] Impact Coatings AB, Westmansgatan 29, SE-582 16 Linköping, Sweden

ARTICLE INFO

Article history:
Received 15 May 2014
Accepted in revised form 27 August 2014
Available online 6 September 2014

Keywords:
First-principles calculations
Thin films
Ti-C
Silicon
Physical vapor deposition (PVD)

ABSTRACT

Ti-Si-C thin films with varying Si content between 0 to 10 at.% were deposited by DC magnetron sputtering from elemental targets. The effects on microstructure and lattice parameters were investigated using x-ray diffraction, x-ray photoelectron spectroscopy, transmission electron microscopy, and first-principles calculations. The results show that the growth of pure TiC_x onto $Al_2O_3(0001)$ substrates at a temperature of 350 °C yields (111) epitaxial and understoichiometric films with $x \sim 0.7$. For Si contents up to 4 at.%, the TiC_x epitaxy is retained locally. Si starts to segregate out from the TiC_x to column boundaries at concentrations between 1 and 4 at.%, and causes a transition from epitaxial to polycrystalline growth above 4 at.%. Eventually, the top part of the films form a nanocomposite of crystalline TiC grains surrounded by amorphous SiC and C for Si contents studied up to 10 at.%. The results show that Si takes the place of carbon when incorporated in the TiC lattice.

1. Introduction

The interaction between Si and TiC is important for understanding how Ti-Si-C coatings can combine high hardness and low friction [1,2] with good electrical properties [3,4]. The amount of both Si and C in the Ti-Si-C coatings greatly affects their properties and structure [2,5,6]. Depending on the composition, temperature, and type of growth template, the structure of the Ti-Si-C materials can form a solid solution, two- or multiphase materials, nanocomposite or nanolaminate structures. For a given composition and high deposition temperature (above ~700 °C), the material system will form Ti_3SiC_2, a so called MAX phase. MAX phases are a group of inherently nanolaminated materials consisting of an early transition metal (M), a group A element and either C and/or N (X) [7]. Ti_3SiC_2 has an interesting combination of metallic and ceramic properties such as good electrical and thermal conductivity, together with corrosion and heat resistance [8,9]. However, the high deposition temperature for Ti_3SiC_2 is prohibitive for deposition onto several industrially relevant substrates, e.g., steel and Cu.

If Ti-Si-C is deposited at temperatures below ~700 °C, Ti_3SiC_2 does not form because of the limited diffusivity of the atoms preventing them from partitioning in the relatively large unit cell (~17.7 Å c-axis) [4,9]. Down to ~400 °C, the dominant crystalline phase is instead TiC_x in the NaCl (B1) structure, while $Ti_5Si_3C_x$ and different titanium-silicides have also been observed in XRD [5,9,10]. If the temperature is decreased further (below ~400 °C), TiC_x becomes the only crystalline phase and typically forms a nanocomposite that consists of nanocrystalline TiC_x (nc-TiC_x), surrounded by an amorphous matrix of predominantly SiC (a-SiC) and C (a-C) [3,9–11]. The solubility of Si in the cubic TiC is low (less than ~1–2 at.%) [12,13]. At low deposition temperatures, out diffusion of Si is hindered and more Si can be incorporated into the TiC structure [9]. Si has been suggested to substitute for either C [14,15] or Ti [16–18]. However, a deeper understanding of how Si would be incorporated in the NaCl-structured TiC_x phase as well as how Si segregates to form another crystalline phase or composite material at low temperatures is lacking. Here, we use x-ray diffraction (XRD), x-ray photoelectron spectroscopy (XPS), transmission electron microscopy (TEM), and first-principles calculations to investigate these phenomena by gradually incorporating Si into a model system of epitaxial TiC_x ($x \sim 0.7$) resulting in thin films that, with increasing Si content in the range 0–10 at.%, goes from epitaxial Ti(Si,C) to a nanocomposite with nc-TiC_x/a-SiC/a-C.

2. Experimental and computational details

Ti-Si-C thin films were deposited using DC magnetron sputtering in a vacuum system with a base pressure of the order of 10^{-7} Pa from three elemental targets onto $Al_2O_3(0001)$ wafer substrates. The sputtering process was operated in current control mode. The targets were 75-mm-diameter Ti (99.995% purity) and graphite (99.999%), and 50-mm-diameter Si (99.999%, p-doped 0.005–0.020 Ω·cm). The Si target was facing the substrate with a target to substrate distance of 155 mm. The Ti and graphite targets were positioned 180 mm from the substrate at an angle of 35°. The deposition system is further described elsewhere [9]. The substrates were cleaned with acetone and isopropanol in an ultrasonic bath prior to the depositions. During the depositions, the substrate temperature was kept constant at 350 °C in an Ar atmosphere at a pressure of 0.5 Pa. A substrate bias of −50 V was applied. Starting from epitaxial TiC_x without Si, a series of films with different Si content

---

[*] Corresponding author. Tel.: +46 13288977.
E-mail address: olote@ifm.liu.se (O. Tengstrand).

http://dx.doi.org/10.1016/j.surfcoat.2014.08.064
0257-8972/

between 0 and 10 at.% was deposited (cf. Table 1). The TiC was chosen understoichiometric around C/Ti ~0.7 in order to avoid an excess of C that could segregate around the TiC_x grains at $x \gtrsim 0.7$ [5,13].

X-ray diffraction (XRD) θ–2θ scans, pole figures, and strain measurements ($\sin^2(\psi)$ method) were obtained using a Cu Kα x-ray source. For the pole figures, point focus was used together with 2 × 2 mm crossed slits and a parallel-plate collimator as primary and secondary optics, respectively. The same setup was used for the strain measurements. Since epitaxy does not allow the same peak to be observed at different ψ angles, multiple peaks were used in the strain measurement. From each peak, the lattice parameter was calculated and plotted against the corresponding $\sin^2(\psi)$ value. A linear curve was then fitted to the data points using the least square method. The strain-free lattice is given for $\sin^2(\psi) = 0.32$, which corresponds to a Poisson ratio of 0.19 (TiC) [19].

Using a FEI Tecnai G2 TF 20 UT instrument with a field-emission gun operated at an acceleration voltage of 200 kV, transmission electron microscopy (TEM) images and selected area electron diffraction (SAED) patterns of cross-sectional and plan-view specimens were obtained for a selected set of samples. Energy-dispersive x-ray spectroscopy (EDX) was used for elemental mapping in scanning TEM (STEM) mode. The cross-sectional specimens were prepared by mechanical polishing down to ~50 μm while the plan-view specimens were mechanically polished from the backside down to ~70 μm and then dimpled to a thickness of ~30 μm. All specimens were then ion-milled in a Gatan precision ion polishing system (PIPS) using 5 keV Ar^+ ions. As a final step, the specimens were polished with 2 keV Ar^+ ions.

The elemental composition of the coatings was determined from x-ray photoelectron spectroscopy (XPS) depth profiles using a Physical Systems Quantum 2000 spectrometer with monochromatic Al Kα radiation and rastered sputtering over an area of 1 × 1 mm^2 using 1 keV Ar^+-ions. To obtain the correct sensitivity factors for composition, the spectra were calibrated against elastic recoil detection analysis (ERDA) measurements made on a selected subset of the samples. The high-resolution XPS spectra were acquired after 30 min of sputtering using 200 eV Ar^+ ions. The binding energy has been calibrated with Ag and Au reference samples. All measurements were performed using an analysis area with a diameter of 200 μm.

First-principles density functional theory calculations were performed using the projector-augmented wave method [20] as implemented in the Vienna ab initio simulation package (VASP) [21,22]. The generalized gradient approximation (GGA) [23] was used for exchange-correlation effects. Supercells based on a 3 × 3 × 3 repetition of the conventional TiC cubic unit cell (108 Ti and 108 C atoms) were used as a starting point to derive input structures for modeling low concentrations of Si as a solid solution on the Ti and C sublattices, respectively. The special quasi-random structure (SQS) approach [24] was used to model a disordered distribution of carbon site vacancies together with different concentrations of Si on the carbon sublattice. For this purpose, three-component SQS supercells were created with the following compositions: $Ti(C_{0.75}Si_{0.037}Vac_{0.213})$ with ~2.1 at.% Si, $Ti(C_{0.75}Si_{0.074}Vac_{0.176})$ with ~4.1 at.% Si, and $Ti(C_{0.676}Si_{0.074}Vac_{0.25})$ with ~4.2 at.% Si. To model a Si solid solution on the Ti sublattice in the presence of disordered vacancies on the carbon sublattice, the starting point was a $TiC_{0.75}$ SQS, where either 1 or 8 Ti atoms chosen randomly were replaced by Si atoms. To obtain good statistics, averaging over 5 different Si distributions were performed in each case. The compositions obtained in this way were $(Ti_{0.991}Si_{0.009})(C_{0.75}Vac_{0.25})$ and $(Ti_{0.926}Si_{0.074})(C_{0.75}Vac_{0.25})$ with ~0.5 and ~4.2 at.% Si, respectively. A Monkhorst-Pack grid of 3 × 3 × 3 k-points and a plane wave energy cutoff of 400 eV were used in the calculations. The obtained energies as a function of lattice spacing were fitted to a modified Morse function [25] from which equi/librium lattice spacings and energies were obtained.

Table 1
Composition of the films determined from XPS depth profiles.

Si target current [mA]	Si [at.%]	Ti [at.%]	C [at.%]	O [at.%]	x in TiC_x [−]
0	0	58	42	0	0.67
10	1	58	41	0	0.65
20	4	57	39	0	0.63
30	6	55	37	2	0.57
40	8	54	35	3	0.50
50	10	52	35	3	0.51

3. Results

Table 1 shows the thin film sample compositions as determined by XPS. The C-to-Ti ratio (x) in the TiC_x grains was calculated from XPS data by excluding the amount of C binding to elements other than Ti in the C1s spectra (cf. Fig. 6b). From the table, we see that the Si content varies from 0 to 10 at.%. With increasing Si content, the TiC_x understoichiometry also increases. We can also see that the films contain contamination of O by less than 2–3 at.%, with the higher content for films with more than 4 at.% Si. The source of oxygen is discussed in Section 4.1.

XRD θ–2θ scans in the range of $2\theta = 10$–$100°$ (data not shown) demonstrated that all films have a crystalline TiC phase with <111> out-of-plane growth texture. No other crystalline phases than TiC could be found. Fig. 1a shows θ–2θ scans for the TiC 111 peak. As a general trend, decreased peak intensity for increased Si content can be seen together with a peak broadening. The 111 peak first shifts to lower 2θ values with increasing Si content going from 35.88° to 35.70° at 0 and ~4 at.% Si, respectively. For higher Si content, the peak moves back towards higher 2θ values. Fig. 1b shows the measured shifts in the lattice parameter of TiC. To exclude the contribution from strain, $\sin^2(\psi)$ measurements were made and the strain-free lattice parameter was calculated for the different films. Although the difference in lattice

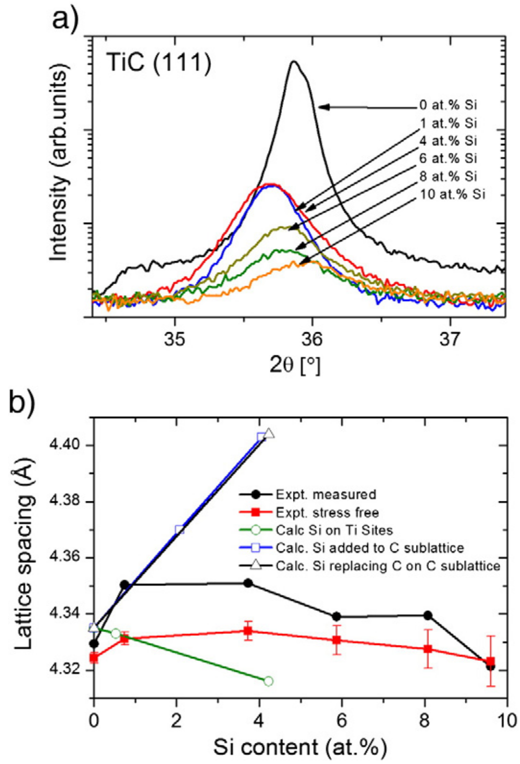

Fig. 1. (a) X-ray diffractogram of the TiC (111) peak for 6 different films with increasing Si content and (b) comparison between theoretical calculations and experimental measurements (present films) of the lattice parameter. The error bars correspond to the calculated standard deviation in lattice parameter for each composition.